Acta Cryst. (1999). A**55**, 901–907

Dynamical scattering and electron diffraction from thin polymer lamellar crystals – poly(*tert*-butylethylene sulfide)

Douglas L. Dorset,[a]* Philippe Dumas,[b] Laurent Cartier[c] and Bernard Lotz[c]

[a]*Electron Diffraction Department, Hauptman–Woodward Medical Research Institute, 73 High Street, Buffalo, NY 14203-1196, USA,* [b]*Laboratoire de Chimie Macromoleculaire, ENSCMu, ICSI-CNRS, 3 rue A. Werner, F-68093 Mulhouse CEDEX, France, and* [c]*Institut Charles Sadron, EAHP-ULP, CNRS, 6 rue Boussingault, F-67083 Strasbourg CEDEX, France. E-mail: dorset@hwi.buffalo.edu*

(*Received 25 August 1998; accepted 19 March 1999*)

Abstract

Strong violations of Friedel symmetry are observed in *hk*0 electron diffraction patterns from lamellar crystals of poly(*tert*-butylethylene sulfide) obtained at 120 kV. These deviations are largely explained by a multislice dynamical scattering calculation based on the crystal structure model. Further improvement is found when a secondary scattering component is added, in keeping with a perfect crystallite thickness less than that of the lamellar thickness. Despite the multiple-scattering perturbations, the frustrated chain packing can still be determined by direct methods followed by Fourier refinement. However, the Friedel-related intensities must be averaged before calculation of normalized structure factors.

1. Introduction

In recent years, there has been a significant revival of quantitative structure analyses based on experimental electron diffraction intensity data sets (Dorset, 1995*a*), partially vindicating pioneering Russian efforts (Vainshtein *et al.*, 1992). The multiple-beam dynamical scattering theory for electrons from thin crystals (Cowley, 1995) has been utilized to design optimal conditions for data collection, *i.e.* minimizing the specimen thickness and by choice of an appropriate electron wavelength. Direct methods for structure analysis have been shown to require merely that observed intensities conform to a 'quasi-kinematical' approximation rather than a strict adherence to the single-scattering limit (Dorset, 1995*b*). This means that the experimental Patterson function calculated from observed intensities should overlap sufficiently with the actual autocorrelation function of the crystal structure. Hence, there is enough information remaining in the intensity data to determine the crystal structure.

While these approximations often may not be questioned when electron crystallographic methods are applied to organics, or any other materials composed of light atoms, successful application of *ab initio* structure determination (including the direct interpretation of symmetry-averaged images) to inorganics has been a surprising development. Echoing the successful analysis of early Russian oblique texture patterns (Vainshtein *et al.*, 1992), new precession techniques (Vincent & Midgley, 1994) for collection of true integrated intensities from crystalline nanoareas have recently allowed the structure of an aluminium–iron alloy to be determined routinely by automated direct methods (Gjønnes *et al.*, 1998).

Concerns about dynamical scattering perturbations to diffraction intensities (or image details) from inorganic crystals had, for a time, impeded significant development of electron crystallographic techniques. However, in an almost complete reversal of these reservations, an entirely kinematical approach to the structure analysis of inorganics has been proposed in recent years (Zou, 1995; Weirich *et al.*, 1996). An impressive analysis of incommensurately modulated high-T_c superconductors can be cited as an example where such methods have been extended to multiple dimensions (Fan *et al.*, 1997), results that have been confirmed by a separate X-ray determination.

It has been postulated, for example, that more error might result from a misjudgment of the objective-lens phase-contrast transfer function than the dynamical interactions themselves (Klug, 1978–1979). On the other hand, eloquent demonstrations of dynamical scattering effects have been made when the physical measurement of phase invariants has actually facilitated determination of crystallographic phases (Kambe & Moliere, 1970; Spence & Zuo, 1992). Also, incorporation of multiple-beam dynamical scattering calculations into structure refinement illustrates how the structural model might converge to the measured data set (Zandbergen *et al.*, 1997; Dorset, 1997). The influence of dynamical interactions on inorganic structure determinations by direct phasing methods has also been discussed (Sinkler & Marks, 1999).

In numerous organic structures determined from electron diffraction intensities, it has been tacitly assumed that an initial kinematical assumption would

lead to an almost correct structural model, provided that sufficient care was taken to collect a self-consistent set of intensities that also sampled the most intense part of the reciprocal lattice (Dorset, McCourt, Li & Voigt-Martin, 1998). However, this approach has never implied the fundamental correctness of the kinematical model itself. For example, measurable dynamical scattering has been demonstrated from 48 Å-thick paraffin monolayer crystals with 1000 kV electrons (Dorset, 1976), refuting previous claims of a 'kinematical limit' at high voltage (Honjo & Kitamura, 1957).

In the following, the marked violation of Friedel symmetry for some reflections observed in the electron diffraction pattern from a thin polymer lamellar crystal is described. The origins of this effect are shown to conform to the multiple-beam model for dynamical scattering and possibly to contain some structural information.

2. Data and calculations

2.1. *Polymer data*

As described recently (Cartier, Spassky & Lotz, 1998), *hk*0 electron diffraction patterns were obtained at 120 kV by selected-area methods from crystalline lamellae of optically active poly(*tert*-butylethylene sulfide) (PTBES) using a Philips CM-12 electron microscope. The monomer was synthesized from *R*(−)-3,3-dimethyl-1,2-butanediol passing through the cyclic carbonate intermediate, which was reacted with potassium thiocyanate at 473 K. Polymerization was initiated by $ZnEt_2/H_2O$ (1:1) and run in toluene solution at room temperature (Dumas *et al.*, 1972). This sample was later used for X-ray structure determination (Matsubayashi *et al.*, 1977) as well as the electron diffraction structure analysis (Cartier, Spassky & Lotz, 1998). Characteristic triangular microcrystals (Cartier *et al.*, 1997) were originally grown within thin cast films. (Epitaxic orientation was also possible on benzylpenicillin but, while the orthogonal view onto the chain axes was important for the initial structure determination, these data will not be considered in this paper.) The unit cell was proposed to be $P3_1$ with $a = 16.91$, $c = 6.50$ Å, with three unique molecules in the unit cell (also with an ambiguity of mixed 'up' and 'down' directions of the chain for any given site). A chain packing model was constructed from geometrical considerations, starting with an energetically stable helical chain conformer, using *Cerius*[2] (Molecular Simulations, Waltham, MA, USA), also minimizing the packing energy in the unit cell. As shown in the potential map calculated from the averaged observed amplitudes and model-derived crystallographic phases (Fig. 1), this corresponded to a 'frustrated' chain packing of the type observed previously for isotactic poly(propylene) in the β-phase (Lotz *et al.*, 1994) and several other polymers (Cartier, Okihara & Lotz, 1998; Cartier & Lotz, 1998; Okihara *et al.*, 1998). This means that the three unique chains have different azimuthal settings in the unit cell so that a simpler unit cell with just one unique chain setting cannot explain the observed diffraction data. Atomic coordinates were given in an earlier paper by Cartier, Spassky & Lotz (1998).

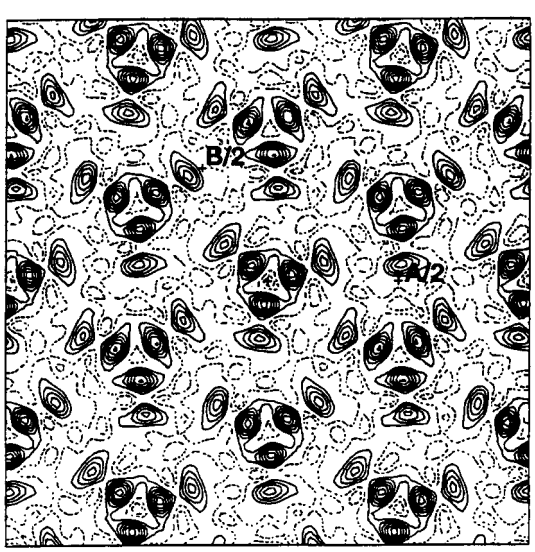

Fig. 1. Chain packing of PTBES observed in a potential map calculated from averaged $|F_{obs}|$ and with crystallographic phases taken from the structural model of Cartier, Spassky & Lotz, (1998).

In this study, intensity data were re-measured from the *hk*0 electron diffraction pattern from scans through the spot profiles, as if a flat bed densitometer had been used. An approximation of the integrated intensity was made by fit of a triangle to the peak profile. A few peaks where the intensity scale had been somewhat saturated were estimated by extending the long sides of the triangle to where they intersect. As usual, no Lorentz correction was made to these data (Dorset, 1995*a*). From these compilations, it was found, as also shown in the original study (Cartier, Spassky & Lotz, 1998), that several strong reflections gave quite different Bijvoet pairs, *e.g.* (140) and ($\bar{1}\bar{4}0$), as well as (410) and ($\bar{4}\bar{1}0$). Obviously, these differences are not explained by a kinematical diffraction model. A Wilson (1942) plot based on averaged Friedel pairs indicated the overall temperature factor to be $B = 0.0$ Å^2. This non-physical value for the Debye–Waller factor is another commonly observed indicator of multiple-beam interactions (Dorset, 1995*a*).

2.2. *Dynamical calculations*

Starting with the atomic coordinates from the original structure determination (Cartier, Spassky & Lotz, 1998), multiple-beam dynamical scattering calculations (Cowley, 1995, pp. 209–253) were carried out on a VAX

Table 1. *Observed and calculated structure factors for PTBES*

MS: $|F_{calc}|$ after multislice calculation. SS: $|F_{calc}|$ after multislice and secondary scattering corrections.

*hk*0	$\lvert F_{obs}\rvert$	MS	SS	*hk*0	$\lvert F_{obs}\rvert$	MS	SS
030	2.23	2.68	2.55	$\bar{2}\bar{6}0$	0.28	0.21	0.26
$0\bar{3}0$	2.14	2.43	2.32	$\bar{3}10$	0.51	0.39	0.45
060	1.46	1.95	1.86	$\bar{3}\bar{1}0$	0.44	0.44	0.49
$0\bar{6}0$	1.49	1.46	1.42	320	0.39	0.28	0.37
110	1.78	1.92	1.86	$\bar{3}\bar{2}0$	0.66	0.56	0.58
$\bar{1}\bar{1}0$	1.92	1.91	1.85	330	0.94	0.41	0.68
120	0.90	0.80	0.78	$\bar{3}\bar{3}0$	0.93	0.57	0.77
$\bar{1}\bar{2}0$	0.75	0.88	0.85	340	0.54	0.45	0.46
130	0.49	0.39	0.45	$\bar{3}\bar{4}0$	0.30	0.40	0.42
$\bar{1}\bar{3}0$	0.53	0.44	0.48	350	0.36	0.23	0.27
140	1.45	1.06	1.10	$\bar{3}\bar{5}0$	0.22	0.36	0.37
$\bar{1}\bar{4}0$	0.51	0.44	0.65	410	0.66	0.18	0.51
150	0.28	0.21	0.28	$\bar{4}\bar{1}0$	1.15	1.08	1.12
$\bar{1}\bar{5}0$	0.47	0.41	0.44	420	0.26	0.00	0.23
160	0.35	0.09	0.19	$\bar{4}\bar{2}0$	0.46	0.62	0.61
$\bar{1}\bar{6}0$	0.47	0.16	0.21	440	0.53	0.54	0.59
170	0.79	0.32	0.48	$\bar{4}\bar{4}0$	0.66	0.43	0.51
$\bar{1}\bar{7}0$	0.91	1.19	1.15	510	0.48	0.61	0.61
210	0.98	1.10	1.04	$\bar{5}\bar{1}0$	0.32	0.39	0.43
$\bar{2}10$	0.82	1.04	1.00	520	1.22	1.13	1.12
220	1.19	0.64	0.81	$\bar{5}\bar{2}0$	1.32	1.36	1.31
$\bar{2}\bar{2}0$	1.08	0.62	0.79	530	0.28	0.71	0.68
230	0.66	0.69	0.69	$\bar{5}\bar{3}0$	0.37	0.51	0.51
$\bar{2}30$	0.35	0.23	0.34	610	0.47	0.24	0.28
240	0.57	0.54	0.55	$\bar{6}\bar{1}0$	0.32	0.24	0.30
$\bar{2}\bar{4}0$	0.28	0.56	0.57	620	0.33	0.33	0.34
250	1.44	1.46	1.40	$\bar{6}\bar{2}0$	0.24	0.13	0.19
$\bar{2}\bar{5}0$	1.25	1.04	1.04	710	0.99	0.79	0.81
260	0.47	0.00	0.17	$\bar{7}\bar{1}0$	0.64	0.44	0.56

workstation with programs originally obtained from Arizona State University. The slice thickness was chosen to be the *c* length of the unit cell, justified later by preservation of 92.83% of the total scattering energy within the 1.0 Å limit set for the multislice calculations up to 195 Å-thick crystals (30 slices). The calculation involved 769 coefficients.

These calculations were tested later against a more rigorous simulation carried out to 3 $Å^{-1}$ resolution with the multislice programs available on the *Cerius*^{2} software package (on a Silicon Graphics R10000 UNIX workstation). Calculations were compared where the unit-cell *c* axis was divided into one or six slices. There was no great difference between the results for any of the simulations carried out in this study to total crystal thicknesses beyond the limits considered. The greatest difference (isotactic polypropylene at lower voltage) in terms of a residual was R = 0.04. For the sulfur-containing polymer, the difference was less than R = 0.02. These residuals are much lower than those found when selected-area diffraction intensities from an organic crystal are combined to assemble a data set (Dorset, McCourt, Li & Voigt-Martin, 1998). Therefore, the differences in the simulations are insignificant.

2.3. *Direct phase determination*

After calculation of normalized *hk*0 structure factors from averaged (often dissimilar) Friedel intensities, Σ_{1^-} and Σ_{2^-} three-phase invariants (Hauptman, 1972) were generated and, from them, a convergence procedure was used to find the most effective means for generating the most number of phase predictions *via* the Sayre (1952) equation from the least set of defining reflections. In this space group, all reflections with $h - k = 3n$ are seminvariants and could not be used for origin definition (Rogers, 1980). Thus, the value of 640 was chosen to define the origin. Two other reflections were selected as algebraic unknowns and one seminvariant reflection was assumed to be chosen *a priori* as a trial enantiomorph selector.

3. Results

3.1. *Dynamical scattering calculations*

The multislice calculations explain the observed breakdown of Friedel's law. However, the optimal match requires that $F_{\bar{h}}$ from the dynamical calculation should be substituted for F_h and *vice versa*. This means that the chirality of the model should be inverted, a result illustrating a positive aspect of exploiting dynamical data from polar projections. (The absolute molecular configuration was unknown when the polymer model was constructed.) The ratio of the two predicted Friedel-related structure-factor amplitudes, $|F_h|/|F_{\bar{h}}|$, for some of the major reflections is shown in Fig. 2 in a sequence of crystal thicknesses. Observed values of these ratios indicate that the true coherent thickness of the sample for dynamical scattering is less than the ~100 Å often found for solution-crystallized polymer lamellae. While various thicknesses can be tried, as well as thermal parameters, a favorable comparison, R = 0.24 (Table 1),

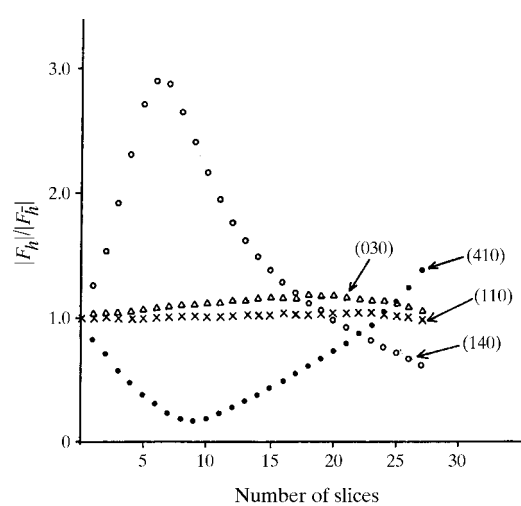

Fig. 2. Plot of $|F_h|/|F_{\bar{h}}|$ ratios in representative *hk*0 reflections at various slice intervals from a multislice dynamical calculation.

is made for a coherent scattering thickness of 58.5 Å when $B = 3.0$ Å^2 for all atoms. This can be compared with $R = 0.29$ for the kinematical model. In general, the fit of a scattering model is worse for trial thicknesses below and above this value. Most importantly, the multislice calculation correctly predicts which specific reflections should give large Bijvoet differences and which should not.

It is also clear that, if the coherent thickness for dynamical scattering is less than the lamellar thickness, layer defects should occur in the structure. This would imply that secondary scattering (Cowley *et al.*, 1951) should also be important where $I' = I + mI * I + \ldots$, where $*$ denotes convolution, is the measured intensity containing a weighted convolution due to strong reflections from upper layers behaving as ancillary primary beams. In this calculation, the I values were assumed to be the asymmetric dynamical values from the multislice calculation. With a modest amount of secondary scattering, the R value can be reduced to 0.17 (Table 1). This noncoherent form of multiple scattering (Cowley, 1995, p. 374) is another complication often experienced in selected-area diffraction experiments on organic crystals (Dorset, 1995*a*), arising from their inherent imperfection.

3.2. *Direct structure determination*

The Bijvoet differences should not be emphasized when solving the structure by traditional direct methods if a kinematical model is assumed. Thus, all Friedel-related reflections were averaged to give a single value for I_{hk0} and its Friedel mate. For the 50 Σ_2 invariants with the largest value of $A = (2/N^{1/2})|E_h E_k E_{-h-k}|$, the average value of the invariants using the phase values calculated from the structural model is $1.4 \pm 78.5°$ when a value of 0° was predicted.

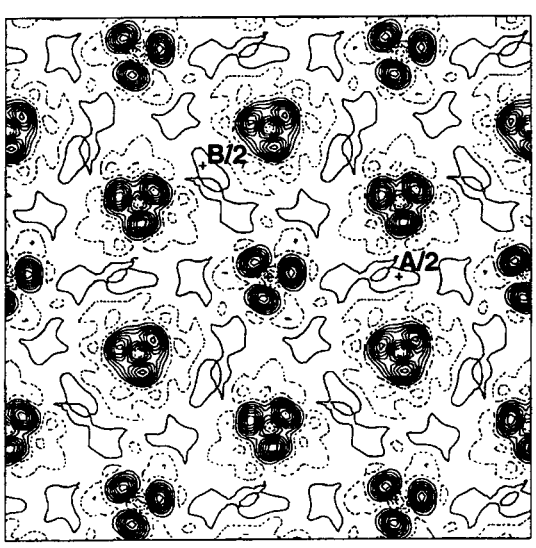

Fig. 3. Test of direct methods *via* the Sayre equation starting with an ideal basis set.

In the first test with the Sayre equation, ideal model phase values were assigned to the 640, 110 and 060 reflections. After the first cycle, in which 14 phases were assigned values, the mean phase error was 38.6°; after the second cycle, assigning all 39 reflections, this error was 54.3°, but only 30° for 14 $|E_h| > 1.0$. The resultant structure calculated from these phases (Fig. 3) could be compared with the map calculated from the model-derived phases (Fig. 1). Note that the 'frustrated' nature of the molecular packing in the unit cell is identified correctly, but only the atoms of the inner part of the polymer chain (containing also S atoms) are visualized clearly.

In a second trial of the Sayre equation, another possible basis set was chosen. The 640 reflection was given its true value to set the origin and the values of 060 and 250 were cycled through phase quadrants as algebraic unknowns, however, restricting 060 to positive 45 and 135°, to set the enantiomorph. This gave phase values for nine reflections, from which trial potential maps were calculated. The most 'peaky' value of $\langle\rho^5\rangle$ for the $|E_h|$ maps (Stanley, 1986) was chosen to indicate the correct basis for a second convolutional cycle. Although the mean phase error for the top 14 reflections was reasonable (34.9°), unique azimuthal orientations of the chain could not be visualized in the potential maps. Moreover, only 38 of the 39 reflections were assigned phase values.

In a third trial, the basis set used before was again selected. The 640 reflection was used to set the origin and the 110 set the enantiomorph, while the values of 060 were cycled through the phase quadrants (±45°, ±135°). After one cycle, 15 reflections were assigned values but the $\langle\rho^5\rangle$ criterion (Stanley, 1986) was not useful for identifying the correct structure. Potential maps calculated from the four phase choices, however, were useful since only one corresponded to a reasonable trimer of blobs for all unique chains in the unit cell. After a second cycle, the potential map (Fig. 4*a*) correctly identified the frustrated nature of the chain packing, even though the overall phase error was 52.5°. (However, the frustrated chain packing was not visible after the first Sayre expansion cycle.) Again, only the inner part of the chain was visualized. This structure could be completed, to find a density close to that of the side chain, by five cycles of Fourier refinement, using a carbon position to model the peripheral glob (Fig. 4*b*). The overall phase error was 49°.

The structure could be completed more efficiently from a Patterson map calculated *via* $(|F_h| - |F_{\bar{h}}|)^2$ terms. By analogy with anomalous scattering (Hendrickson & Ogata, 1997), the dynamical scattering might, conceivably, be modeled by an imaginary scattering factor for the Sr atoms. However, the autocorrelation function

calculated from S-atom positions did not resemble the Patterson function calculated from the Bijvoet differences. What was found from the experimental Patterson was the radial position of the side-chain densities. If carbon positions were placed at this radial distance from the inner sulfur positions, the final map (Fig. 4*c*) closely resembled the one found by Fourier refinement, and the overall mean phase error was 50.3°.

4. Discussion

At first glance, it might be surprising to observe such a strong manifestation of dynamical scattering through a breakdown of Friedel's law in the electron diffraction from an organic structure. It is clear that the polarity of the unit cell and also its projection is largely responsible for this effect (Miyake & Uyeda, 1950), since this is a well known criterion for identifying polar inorganic structures (Goodman & Lehmpfuhl, 1968). Organics containing sulfur exhibit strong dynamical effects, even when the projected density is centrosymmetric. For example, in the study of poly(ethylene sulfide), the sulfur position was correctly identified after direct phasing of *hk*0 data but the lighter carbon position was less accurately found (Dorset & McCourt, 1992). Even with oblique texture data from two thermotropic polymorphs of thiourea (Dvoryankin & Vainshtein, 1960, 1962), where nonsystematic dynamical interactions might be expected to be 'averaged out' by all the sampled crystallite orientations, these perturbations were still strong enough to prevent effective refinement of the structure to be carried out by Fourier techniques. The sulfur positions were found correctly for each polymorph but the lighter atoms were located near their correct positions (Dorset, 1992) only after the data are re-scaled to an average two-beam approximation (Vainshtein & Lobachev, 1956) of the structure factor, *i.e.* $|F_{obs}| = kI_{obs}$.

The breakdown of Friedel's law for a polar space group in an organic substance was also observed (Glaeser & Ceska, 1989) in electron diffraction patterns taken from bacteriorhodopsin (again plane group *p*3) at

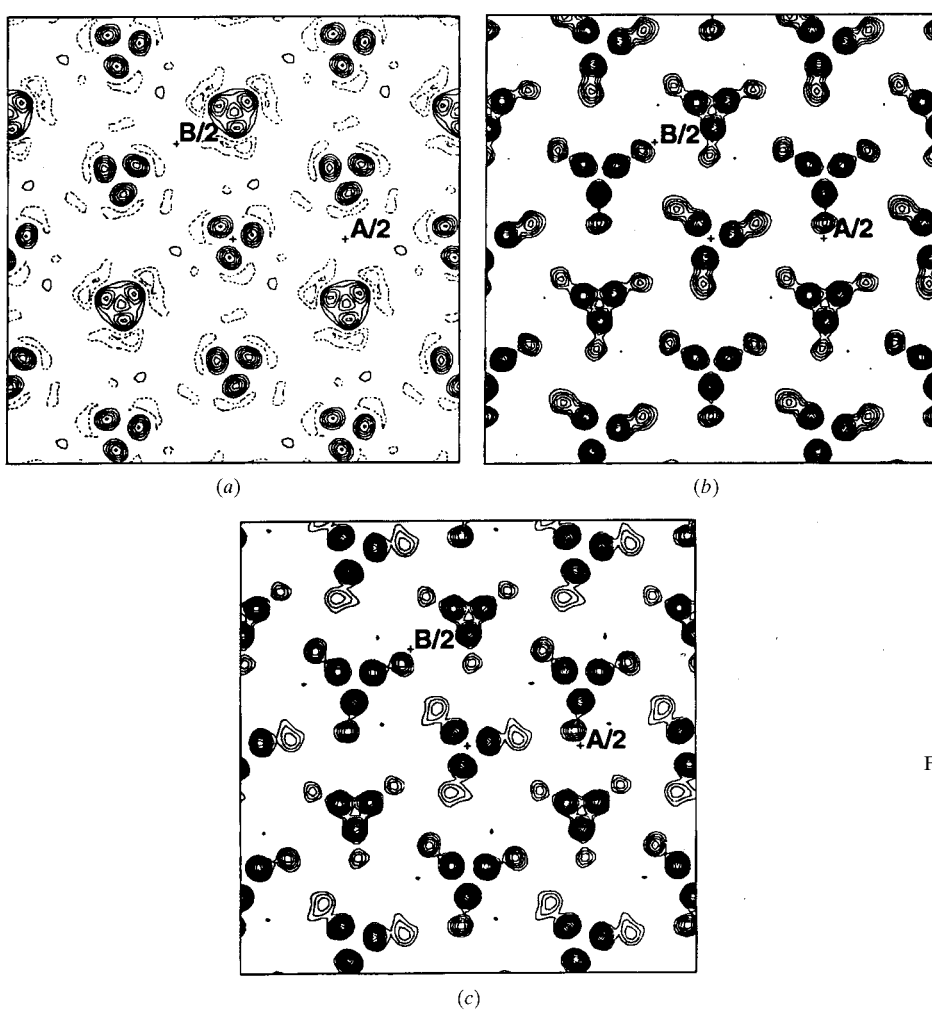

Fig. 4. Test of the Sayre equation, quadrant sampling for an algebraic quantity: (*a*) second cycle, identifiable solution with partial density distribution but correct 'frustrated' aspect of chains; (*b*) potential map after five cycles of Fourier refinement; (*c*) side-chain positions located by 'dynamical' Patterson synthesis, based on Friedel differences $(|F_h| - |F_{\bar{h}}|)^2$.

20 kV (but not 120 kV). While the individual intensity differences were also large, there was less deviation from the kinematical model if the Friedel mates were averaged, as also found for this polymer.

The coherence thickness for dynamical scattering does not correspond to the lamellar thickness for this sulfur-containing polymer. In fact, the value is only about one-half of the typical lamellar thickness for polymers. As stated above, this implies that there are, on average, enough imperfections in the lamellar stem packing, perhaps due to conformational defects and embedded chain terminations, to restrict the perfect crystallite size. The improved fit of the observed structure factors when a small amount of secondary scattering is added to the model is again consistent with a defect model. It has also been reported that dynamical scattering calculations for other polymer data sets generally gave a best fit at a thickness less than the actual lamellar value (Moss & Dorset, 1982).

If dynamical scattering can be limited to a point where it just begins to be expressed, then this could be an ancillary source of phase information (Moodie, 1965). We have already explored the idea of the dynamical effect approximated by a complex scattering factor, as once attempted to explain electron diffraction from a crystal by a pseudokinematical theory (Hoerni, 1956; Kainuma & Lipscomb, 1961). In this case, the pseudokinematical model was proposed to mimic the dynamical theory from very thin crystals. While the analogy to anomalous scattering does not hold, as also found for high-index reflections in the earlier study (Hoerni, 1956), there appears to be structural information contained in the Patterson formed from Bijvoet differences, if not the expected heavy-atom scattering.

Perhaps specific joint phase invariants utilizing dynamically induced amplitude differences in Friedel pairs (Hauptman, 1982) could be formulated to yield more accurate phase values by direct methods. This view is supported by a separate analysis of three- and four-phase structure invariants. Given Σ_2 three-phase invariants (Hauptman, 1972), distinct values of I_h and $I_{\bar{h}}$ were used to calculate $|E_h|$ and $|E_{\bar{h}}|$. When $|A^+ - A^-|/|A^+ + A^-|$, calculated for any triple and its Friedel-related sum, differs by more than a certain threshold value, it is more accurate to add a $\pm 90^\circ$ phase shift to the triple estimate. However, it is difficult to predict the direction of this shift *a priori*. The positive quartet invariants (Hauptman & Green, 1976) are more strongly affected. Very few of those with the largest $B=(2/N)\times|E_hE_kE_lE_m|$ are correctly predicted. Those with large values of $|B^+ - B^-|/|B^+ + B^-|$ should be shifted by almost 180° to give accurate phase estimates. On the other hand, when Bijvoet differences were generated from 20 to 120 kV by a multislice calculation for a polar hydrocarbon polymer, untwinned β-phase isotactic poly(propylene) (Dorset, McCourt, Kopp *et al.*, 1998), these differences were not useful for predicting accurate invariant values by the above method. It is apparent that at least one atom in the structure must have a distinctly different Z value for this approach to be effective. In this respect, the phenomenon is analogous to anomalous-scattering experiments.

Research was supported in part by a grant from the National Science Foundation (CHE97-30317) to DLD, which is gratefully acknowledged. Dr Mary P. McCourt is thanked for assistance in carrying out some of the dynamical scattering simulations.

References

Cartier, L. & Lotz, B. (1998). *Macromolecules*, **31**, 3049–3054.
Cartier, L., Okihara, T. & Lotz, B. (1997). *Macromolecules*, **30**, 6313–6322.
Cartier, L., Okihara, T. & Lotz, B. (1998). *Macromolecules*, **31**, 3303–3310.
Cartier, L., Spassky, N. & Lotz, B. (1998). *Macromolecules*, **31**, 3040–3048.
Cowley, J. M. (1995). *Diffraction Physics*, 3rd ed. (rev.). Amsterdam: North-Holland.
Cowley, J. M., Rees, A. L. G. & Spink, J. A. (1951). *Proc. Phys. Soc. (London) Sect. A*, **64**, 609–619.
Dorset, D. L. (1976). *J. Appl. Phys.* **47**, 780–782.
Dorset, D. L. (1992). *Ultramicroscopy*, **45**, 357–364.
Dorset, D. L. (1995*a*). *Structural Electron Crystallography*. New York: Plenum.
Dorset, D. L. (1995*b*). *Acta Cryst.* A**51**, 869–879.
Dorset, D. L. (1997). *Acta Cryst.* A**53**, 356–365.
Dorset, D. L. & McCourt, M. P. (1992). *Trans. Am. Crystallogr. Assoc.* **28**, 105–113.
Dorset, D. L., McCourt, M. P., Kopp, S., Schumacher, M., Okihara, T. & Lotz, B. (1998). *Polymer*, **39**, 6331–6337.
Dorset, D. L., McCourt, M. P., Li, G. & Voigt-Martin, I. G. (1998). *J. Appl. Cryst.* **31**, 544–553.
Dumas, P., Spassky, N. & Sigwalt, P. (1972). *Makromol. Chem.* **156**, 55–64.
Dvoryankin, V. F. & Vainshtein, B. K. (1960). *Sov. Phys. Crystallogr.* **5**, 564–574.
Dvoryankin, V. F. & Vainshtein, B. K. (1962). *Sov. Phys. Crystallogr.* **6**, 765–772.
Fan, H. F., Wan, Z. H., Li, J. Q., Fu, Z. Q., Mo, Y. D., Li, Y., Sha, B. D., Cheng, T. Z., Li, F. H. & Zhao, Z. X. (1997). *Electron Crystallography*, edited by D. L. Dorset, S. Hovmöller & X. D. Zou, pp. 285–294. Dordrecht: Kluwer.
Gjønnes, J., Hansen, V., Berg, B. S., Runde, P., Cheng, Y. F., Gjønnes, K., Dorset, D. L. & Gilmore, C. J. (1998). *Acta Cryst.* A**54**, 306–319.
Glaeser, R. M. & Ceska, T. A. (1989). *Acta Cryst.* A**45**, 620–628.
Goodman, P. & Lehmpfuhl, G. (1968). *Acta Cryst.* A**24**, 339–347.
Hauptman, H. (1982). *Acta Cryst.* A**38**, 632–641.
Hauptman, H. & Green, E. A. (1976). *Acta Cryst.* A**32**, 45–49.
Hauptman, H. A. (1972). *Crystal Structure Determination. The Role of the Cosine Seminvariants.* New York: Plenum.

Hendrickson, W. A. & Ogata, G. M. (1997). *Methods Enzymol.* **276**, 494–523.
Hoerni, J. A. (1956). *Phys. Rev.* **102**, 1534–1542.
Honjo, G. & Kitamura, N. (1957). *Acta Cryst.* **10**, 533–534.
Kainuma, Y. & Lipscomb, W. N. (1961). *J. Phys. Soc. Jpn*, **16**, 495–500.
Kambe, K. & Moliere, K. (1970). *Adv. Struct. Res. Diffr. Methods*, **3**, 53–100.
Klug, A. (1978–1979). *Chem. Scr.* **14**, 245–256.
Lotz, B., Kopp, S. & Dorset, D. (1994). *C. R. Acad. Sci. (Paris) Ser. II*, **319**, 187–192.
Matsubayashi, H., Chatani, Y., Tadokoro, H., Dumas, P., Spassky, N. & Sigwalt, P. (1977). *Macromolecules*, **10**, 996–1002.
Miyake, S. & Uyeda, R. (1950). *Acta Cryst.* **3**, 314.
Moodie, A. F. (1965). *International Conference on Electron Diffraction and Crystal Defects*, Melbourne, Australia. Paper ID-1. Oxford: Pergamon.
Moss, B. & Dorset, D. L. (1982). *J. Polym. Sci. Polym. Phys. Ed.* **20**, 1789–1804.
Okihara, T., Cartier, L., Alberda van Ekenstein, G. O. R. & Lotz, B. (1998). *Polymer*, **40**, 1–11.
Rogers, D. (1980). *Theory and Practice of Direct Methods in Crystallography*, edited by M. F. C. Ladd & R. A. Palmer, pp. 23–92. New York: Plenum.
Sayre, D. (1952). *Acta Cryst.* **5**, 60–65.
Sinkler, W. & Marks, L. D. (1999). *Ultramicroscopy*, **75**, 251–268.
Spence, J. C. H. & Zuo, J. M. (1992). *Electron Microdiffraction*, pp. 107–125. New York: Plenum.
Stanley, E. (1986). *Acta Cryst.* A**42**, 297–299.
Vainshtein, B. K. & Lobachev, A. N. (1956). *Sov. Phys. Crystallogr.* **1**, 370–371.
Vainshtein, B. K., Zvyagin, B. B. & Avilov, A. S. (1992). *Electron Diffraction Techniques*, Vol. 1. edited by J. M. Cowley, pp. 216–312. Oxford University Press.
Vincent, R. & Midgley, P. A. (1994). *Ultramicroscopy*, **53**, 271–282.
Weirich, T. E., Ramlau, R., Simon, A., Hovmöller, S. & Zou, X. D. (1996). *Nature (London)*, **382**, 144–146.
Wilson, A. J. C. (1942). *Nature (London)*, **150**, 151–152.
Zandbergen, H. W., Andersen, S. J. & Jansen, J. (1997). *Science*, **277**, 1221–1225.
Zou, X. D. (1995). PhD thesis, Stockholm University, Sweden.